Materials Chemistry and Physics 123 (2010) 225–230

Contents lists available at ScienceDirect

Materials Chemistry and Physics

journal homepage: www.elsevier.com/locate/matchemphys

Preparation and catalytic properties of tungsten oxides with different morphologies

Yunfei Bi*, Dadong Li, Hong Nie

Research Institute of Petroleum Processing, SINOPEC, 18 Xue Yuan Road, 100083 Beijing, PR China

ARTICLE INFO

Article history:
Received 17 May 2009
Received in revised form 18 March 2010
Accepted 31 March 2010

Keywords:
Nanostructures
Chemical synthesis
Microstructure
Semiconductors

ABSTRACT

Tungsten oxides with different morphologies including platelet-like sheets, nanobelts, and nanoparticles have been successfully prepared by changing the ions in the synthetic solution. Transmission electron microscopy, X-ray diffraction, Fourier-transform infrared analysis and N_2 adsorption were employed to reveal the morphological evolution, and results show that the morphological evolution can be attributed to the alteration of coordination environment of tungstenic cations contained in the synthetic solution. Furthermore, these products have been applied into hydrodesulfurization measurement to investigate the relationship between the morphologies of tungsten oxides and their catalytic properties. It is concluded that the catalysts originating from nanobelt-like tungsten oxides have highest catalytic activity and excellent selectivity due to their scrolled character and strong metallic edges.

1. Introduction

It is well known that physical and chemical properties of materials strongly depend on their structure, morphology, size, phase, etc [1,2]. Therefore, since the discovery of carbon nanotubes in 1991, nanosized building blocks such as nanorods, nonowires, and nanobelts have attracted great interest due to their exceptional geometric and electronic properties [3]. Over the past decades, transition metal oxides have received increasing attention in the "bottom-up" synthesis of nanomaterials. Amongst them, tungsten oxides are an important family of inorganic materials that have high application potential in various fields such as optchromic, electrochromic, and catalysis [4,5]. Much effort has been devoted to their synthesis and some achievements have been obtained. For example, WO_3 nanorods were synthesized by thermal decomposition of $W(CO)_6$ in oleylamine in the presence of mild oxidant $Me_3NO{\cdot}2H_2O$ [6]. In spite of these thought-provoking works, some challenges are still faced. Firstly, finding a facile and ligand-free approach remains to be needed. Secondly, it is rarely reported to date, to the best of our knowledge, to investigate the morphological evolution. Finally, it is meaningful to study the relationship between the morphology and specific properties such as catalytic activity of hydrodesulfurization (HDS) [7,8].

Herein, we report the facile synthesis of tungsten oxides. Particularly, the morphologies of these oxides are successfully varied by changing the ions in the synthetic solution. Not only is the mechanism of morphology evolution discussed based on the detailed data, but also is the HDS activity of these oxides investigated.

2. Experimental

Typically, 2.1 g of Na_2WO_4 was dissolved in 30 mL deionized water to form a transparent solution. Then the same volume of 1 M HCl solution was added slowly into under magnetic stirring. After half an hour, the suspension was transferred into a Telflon-lined stainless steel autoclave, and then hydrothermally treated at 180 °C for 12 h.

X-ray diffraction (XRD) measurements were carried out between 5° and 65° using a Philips XPERT powder diffractometer with CuK_α radiation (wavelength = 1.54 Å). The morphology was characterized by a Joel 2010 transmission electron microscopy (TEM) operating at 200 kV. Fourier-transform infrared (FTIR) spectra were collected with a NEXUS 470 spectrometer in the range of 400–2000 cm^{-1} using the KBr-pellet method. Brunauer–Emmett–Teller (BET) nitrogen adsorption was measured by Shimadzu-Micromeritics ASAP 2010 instrument.

The as-synthesized oxides were sulfided in situ using an *n*-decane solution containing 5 wt% CS_2 at 360 °C for 3 h, and the flow rate was 0.2 mL min^{-1}. The total pressure was 4.2 MPa (hydrogen, flow rate of 180 mL min^{-1}). Catalytic reaction was firstly measured at 280 °C, and carried out in a high-pressure flow microreactor. Reactant feed was the cyclohexane solution containing 0.45 wt% 4,6-dimethyl dibenzothiophene (4,6-DMDBT). An equivalent amount of decalin was added into the solution as an internal reference for quantitative analysis. The flow rate for the reactant feed was 0.4 mL min^{-1}. The reaction effluents were condensed and analyzed by chromatography equipped with a capillary column (OV-17, 25 m long, 0.25 mm internal diameter). The operation at 300 °C was similar to that above.

3. Results and discussion

3.1. TEM analysis

In the typical procedure, light yellow precipitates appeared gradually while 1 M HCl solution was added dropwise into the

* Corresponding author. Tel.: +86 10 82368324; fax: +86 10 62311592.
E-mail address: beiyf2003@yahoo.com.cn (Y. Bi).

0254-0584/$ – see front matter © 2010 Elsevier B.V. All rights reserved.
doi:10.1016/j.matchemphys.2010.03.086

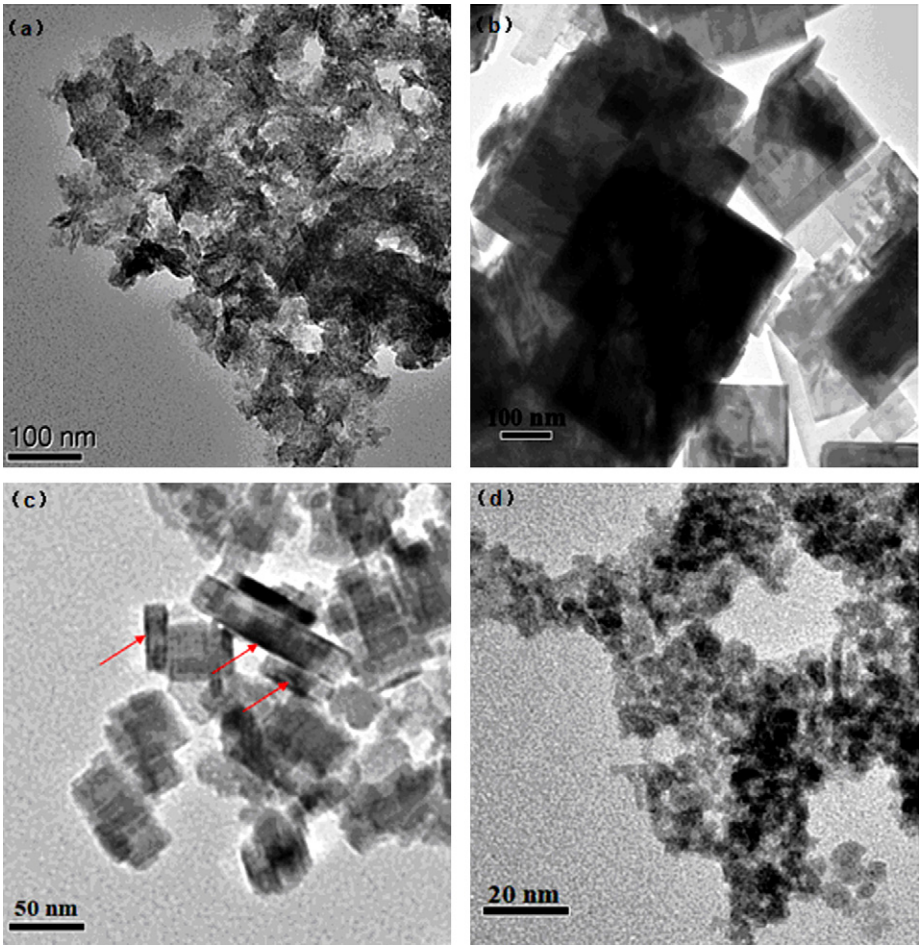

Fig. 1. TEM images of various products: (a) the precipitates formed by acidifying Na_2WO_4 in 1 M HCl solution, without hydrothermal treatment, (b) similar to part (a), but hydrothermal treatment at 180 °C for 12 h, (c) products obtained by acidifying Na_2WO_4 in 1 M H_2SO_4 solution and subsequently hydrothermal treating the resulting suspension at180 °C for 12 h and (d) similar to part (c), but 2 M H_2SO_4 solution.

Na_2WO_4 solution. TEM image reveals that the morphology of products is irregular (Fig. 1a). Interestingly, larger platelets about 200 by 300 nm were obtained when the above suspension was hydrothermal treated at 180 °C for 12 h (Fig. 1b). To gain more information on the morphological change, we varied the concentration of HCl solution from 0.5 to 3 M. Results show that the morphology and the size of products are concentration-independent. However, when 1 M H_2SO_4 instead of HCl is used to acidify Na_2WO_4 solution, the hydrothermal treatment products are nanoplatelets and their size is about 20 by 30 nm (Fig. 1c). Further experiments reveal that these products are concentration-dependent, and can be transformed into nanoparticles with diameter less than 10 nm when the concentration of H_2SO_4 solution reaches 2 M (Fig. 1d). Another evidence for the morphology change is the results of N_2 adsorption. The BET specific surface areas are 8 $m^2\ g^{-1}$ for irregular products, 15 $m^2\ g^{-1}$ for larger platelets, 42 $m^2\ g^{-1}$ for nanoplatelets, and 102 $m^2\ g^{-1}$ for nanoparticles. Based on the BET results it is known that the BET specific surface areas are comparable for irregular particles and larger platelets. The increase of BET specific surface area actually occurs for nanoplatelets and nanoparticles.

It is important to note that a few nanobelts are also observed in Fig. 1c (noted by arrows), which leads one to consider that the conditions being beneficial to form nanobelts may exist in this synthetic solution. When the ions in the synthetic solution are considered, Na^+ and SO_4^{2-} attract more attentions. To reveal the nature of the formation of belt-like morphology we have introduced 10 g of Na_2SO_4 into the suspension obtained by acidifying Na_2WO_4 solution in 1 M HCl. Subsequently, the mixture was hydrothermally treated at 180 °C for various durations. Results are shown in Fig. 2a–d. When the reaction was run for 4 h, short nanobelts and small particles (Fig. 2a) are observed. As the reaction proceeds, small particles disappear and only nanobelts with deficiencies are observed (Fig. 2b), which indicates that the formation of nanobelts is at the cost of small particles. Furthermore, the length of the nanobelts increases with the reaction duration (Fig. 2c). At last, perfect nanobelts about 5 by 200 nm are harvested after the reaction is run for 12 h (Fig. 2d).

3.2. XRD analysis

Fig. 3 shows XRD patterns of the various products. When Na_2SO_4 was not employed, the hydrothermal treatment products are pure WO_3 (JCPDS No. 43-1431, Fig. 3a) whatever the acidification was accomplished by HCl or H_2SO_4. When Na_2SO_4 was employed, the products consist of two crystalline phases (Fig. 3b), $WO_3{\cdot}0.5H_2O$ (JCPDS No. 44-0363) and $WO_3{\cdot}0.33H_2O$ (JCPDS No. 35-1001). The change of crystalline phase indicates that Na_2SO_4 has a great impact on not only the morphology of products, but also their structure.

3.3. FTIR analysis

Considering that XRD pattern only reveals the bulk information of the measured sample, FTIR was also applied to find the subtle difference in as-synthesized products. Indeed, a clear difference is

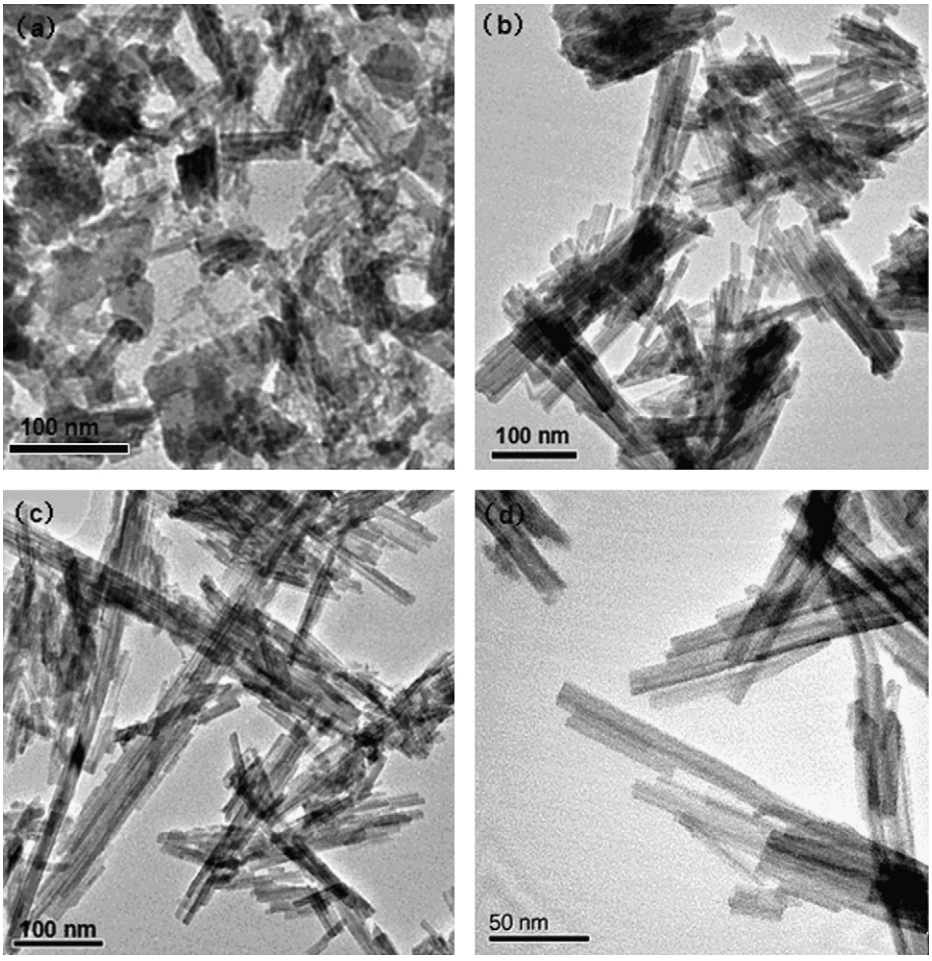

Fig. 2. TEM images of products obtained by hydrothermal treating 10 g Na_2SO_4 and the suspension obtained by acidifying Na_2WO_4 solution in 1 M HCl solution at 180 °C for different durations: (a) 4 h, (b) 8 h, (c) 10 h and (d) 12 h.

shown in Fig. 4. For larger platelets, we only observed the peaks representing W = O stretching vibrations (Fig. 4a). For nanoplatelets and nanobelts, the peaks at 1210 and 1103 cm^{-1}, representing the stretching vibration of SO_4^{2-} [9,10], are observed (Fig. 4b and c), and become stronger in Fig. 4c. The difference indicates the adsorption effect of SO_4^{2-} cations may play an important role on the formation of nanoplatelets and nanobelts.

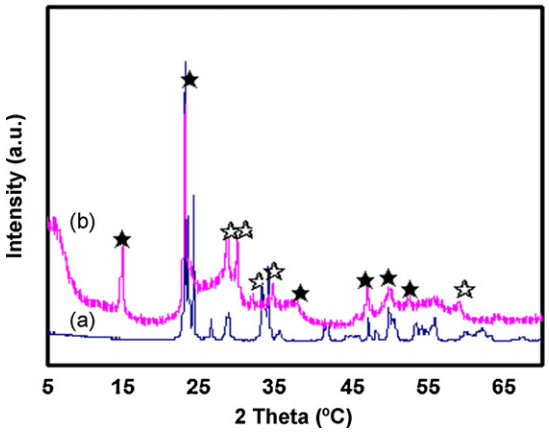

Fig. 3. XRD patterns of various products obtained by hydrothermal treating the suspension obtained by acidifying Na_2WO_4 solution in 1 M HCl solution: (a) without Na_2SO_4, pure WO_3 and (b) with Na_2SO_4, two crystalline phrases: $WO_3 \cdot 0.5H_2O$ noted by (★) and $WO_3 \cdot 0.33H_2O$ noted by (☆).

3.4. Mechanism of morphology evolution

It is well known that tungsten acid precipitates can be formed when Na_2WO_4 solution is acidified [11,12]. The coordinate environment of a W ion in tungstic acid is shown in Fig. 5a [13]. Such coordination results in difficult protonation due to the weak basic-

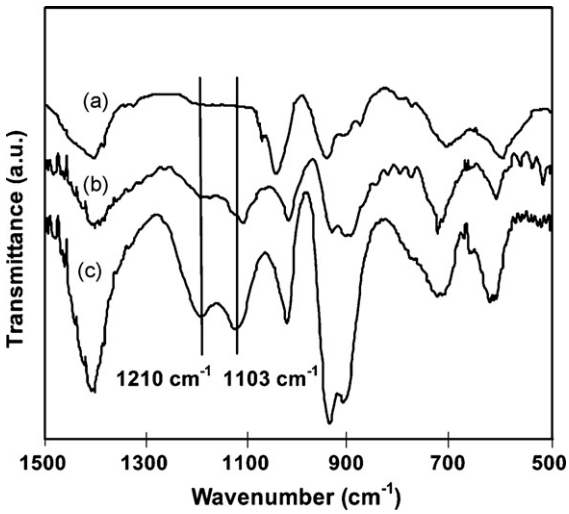

Fig. 4. FTIR spectra of as-synthesized products: (a) larger platelets, (b) nanoplatelets and (c) nanobelts.

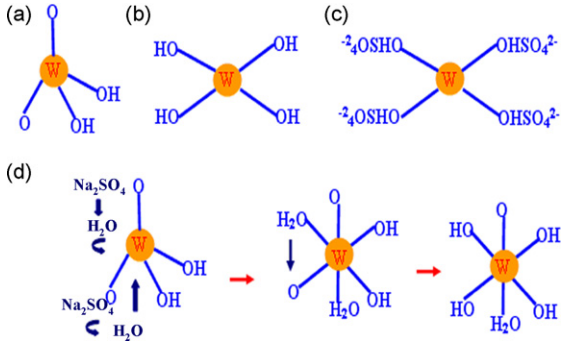

Fig. 5. Schematic diagram of the coordination environment of various products: (a) H_2WO_4 formed after the acidification, (b) protonation due to hydrothermal treatment, (c) SO_4^{2-} anions adsorbing on crystal clusters and (d) coordination expansion due to strong electrostatic repulsions.

ity of strongly bonded terminal W = O. Therefore, in our case the crystalline growth was accomplished by oxolation and olation, which generated irregular morphology.

After the hydrothermal treatment, platelet-like products were formed, which suggests a change of coordination environment. A possible explanation is like this: due to the Brownian motion acceleration and the increased autogenous pressure during hydrothermal treatment, a great part of H^+ cations could become more active, which overcame the weak basicity of terminal W = O. As a result, the protonation was accomplished, and four OH groups were formed (Fig. 5b). Therefore, products grew only by oxolation. It should be noted that the completion of protonation depends only on whether the energy (temperature in our case) is enough, not on the amount of H^+ cations, so it is understandable that the products in Fig. 1b are concentration-independent.

The fact that the size of products decreases when acidification was fulfilled by H_2SO_4 instead of HCl indicates that another limitation effect on the crystal growth of products in addition to the protonation has happened during the hydrothermal treatment. Eventually, not only our FTIR spectra and TEM images, but also past researches have demonstrated that SO_4^{2-} anions had a limitation effect on the crystal growth due to their strong adsorption [14–16]. In our case, SO_4^{2-} anions would adsorb on crystal clusters after protonation was completed (Fig. 5c), and hindered crystal growth by oxolation, which resulted in nanoplatelet. Such limitation effect became more apparent with the increase of the concentration of SO_4^{2-} anions. Once the concentration of SO_4^{2-} anions was high enough, small nanoparticles could be produced.

The structural change due to the addition of Na_2SO_4 suggests that Na_2SO_4 should play important roles. The following fact unveils the nature of such change: Na_2SO_4 will be hydrolyzed in the aqueous solution, and then a microenvironment with rich H_2O molecules is formed [17]. When this solution was hydrothermally treated, coordination expansion led to the formation of sixfold coordinated W^{6+} ion by the nucleophilic addition of two water molecules. However, as the preferred coordination of W^{6+} ion is known to be mono-oxo, the neutral precursor should be $WO(OH)_4(OH_2)$ (Fig. 5d). Under hydrothermal condition, electrostatic repulsions between highly charged W^{6+} ions were stronger, which led to the formation of open structures such as $WO_3 \cdot 0.33H_2O$ [13].

Generally, it is hard to accurately determine the mechanism of the formation of one-dimensional materials. But the experiments targeting to investigate the formation of nanobelts have revealed that this formation was at the cost of nanoparticles. Due to their sizes, nanoparticles can be considered as nanocrystals. The past researches have pointed out that in a supersaturated solution there was a spherical diffusion layer around each nanocrystal, where the concentration of solute keeps unchanged [18–20]. According to the Gibbs–Thompson theory, different growth rates of lateral directions will be occurred due to deficiencies and dangling bonds on the surface of nanocrystals. To keep the spherical diffusion layer, a great quantity of solute was continuously supplied into the layer. As a result, nanocrystals grow into one-dimensional nanobelts. A more beneficial condition for nanobelt growth is that the chemical potential of the solution is higher than that of nanocrystals, so it is not surprising that Na_2SO_4 is more beneficial to the formation of nanobelts than H_2SO_4 since its ionization is easier. Of course, the above results only indirectly show the growth of nanocrystals. To precisely reveal this more powerful tools like in situ characterization are needed.

3.5. Catalytic measurement

Since the morphology of catalysts has an important effect on their catalytic behaviors [7,21], we have tested as-synthesized tungsten oxides with different morphologies. The catalysts obtained by sulfiding as-synthesized oxides are termed as Cata-LP, Cata-NP, and Cata-NB depending on their morphologies (LP: large platelets, NP: nanoplatelets, NB: nanobelts). XRD patterns of these catalysts (data not shown) have no difference and coincide well with typical that of WS_2.

For 4,6-DMDBT, reaction routines have been well developed [8,22]. Generally, the final products include two kinds of hydrocarbons. One is methylcyclohexyltoluene (MCHT) obtained by hydrogenation of aromatic rings (HYD), the other is dimethylbiphenyl (DMBP) obtained by direct desulfurization (DDS). So the selectivity is defined as HYD/DDS = MCHT/DMBP.

The morphologies of sulfided catalysts are shown in Fig. 6, and it can be drawn that catalysts have fallen into pieces after HDS reaction. The close examination of high-resolution transmission electron microscopy (HRTEM) reveals the difference in nanoslabs of these catalysts (Fig. 6a–c, insets). There are long and bent nanoslabs in Cata-LP (Fig. 6a, inset), short and straight in Cata-NP (Fig. 6b, inset), but long and straight in Cata-NB (Fig. 6c, inset).

Fig. 7 shows the catalytic activity (Fig. 7a) and the selectivity of catalysts (Fig. 7b) at 280 and 300 °C. An interesting point is on the catalytic activity and selectivity of Cata-NB. The highest catalytic activity is contrary to the general view due to its long nanoslabs [21,23]. After a close examination, a possible reason has been proposed. We can find that the spacing of nanoslabs in this catalyst (0.68 nm, Fig. 6c, inset) is larger than normal interplanar spacing (0.62 nm). In particular, we observe that the nanoslabs are slightly curved. These evidences show a scrolled character in Cata-NB [24] that can allow H_2 and H_2S to diffuse into the spacing, and then cause a more effective reduction–sulfidation–reduction reaction ($WO_3 \rightarrow WO_2 \rightarrow WS_2 \rightarrow W$) that can produce a numerous of vacancies considered as catalytic sites. The rising catalytic activity of Cata-NB with the increase of HDS reaction temperature supports again the above analysis.

More interestingly, Cata-NB has a more balanced selectivity that is pursued in developing efficient catalysts particular for selective HDS. It is known from the above analysis that the long and straight nanoslabs originated from the one-dimensional morphology. Theoretical calculation has shown that the geometric and electronic configuration of edges exposed by these slabs differed from the bulk, and has strong metallic character [25]. The metallic edges easily bind the reactants containing sulfur. Furthermore, when hydrogen is available at the neighboring edge sites in the form of SH groups, hydrogen transfer reactions may take place, and then aromatic ring hydrogenation may happen [26,27].

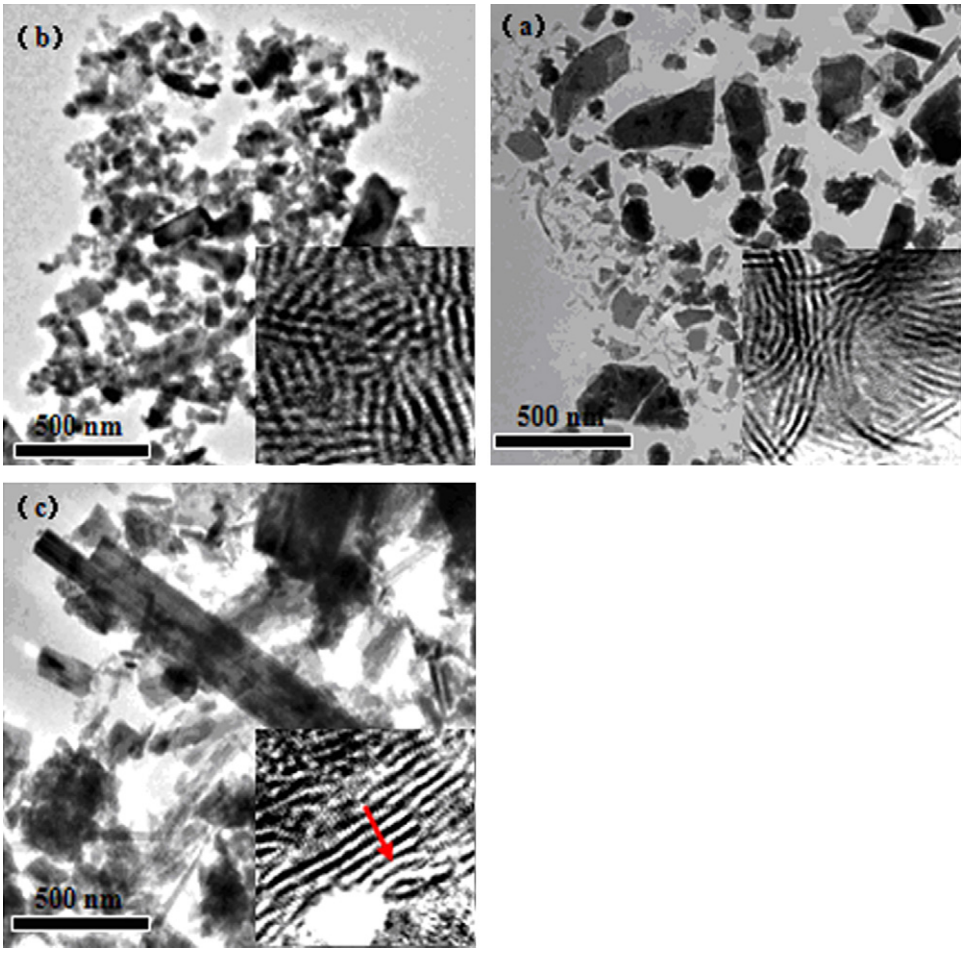

Fig. 6. TEM and HRTEM (insets) images of spent catalysts: (a) Cata-LP, (b) Cata-NP and (c) Cata-NB.

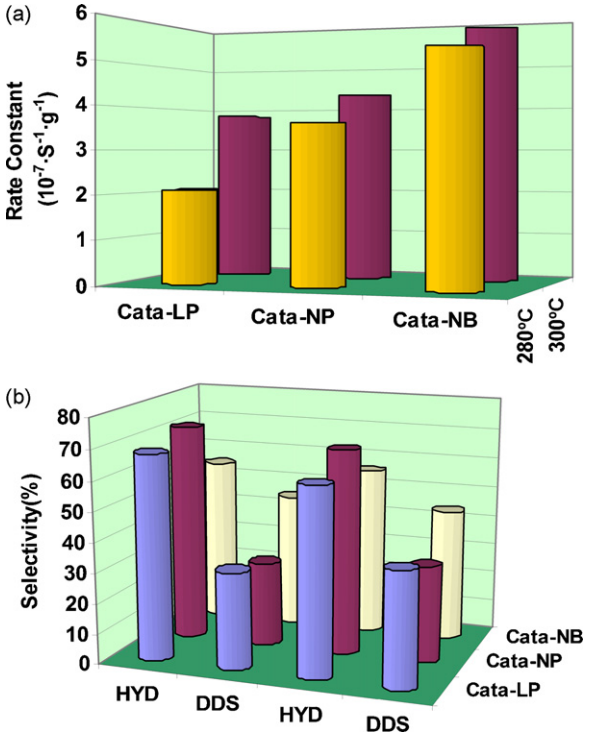

Fig. 7. Catalytic properties of obtained catalysts at 280 and 300 °C: (a) catalytic activity and (b) catalytic selectivity.

4. Conclusion

This paper presents a facile and shape-controlled synthesis of tungsten oxides. In particular, we have varied morphologies of as-synthesized products from different size of platelets to nanobelts, and to nanoparticles. The morphology evolution can be attributed to the change of coordination environment of a W^{6+} ion. When the catalysts obtained by sulfiding as-synthesized tungsten oxides are applied into HDS measurement, an important conclusion is drawn: long and straight nanoslabs can be observed in the catalyst originating from tungsten oxide nanobelts. Such nanoslabs have a scrolled character and strong metallic edges, which promotes the catalytic activity and selectivity. The results open the possibility of not only the analogue preparation, but also the development of higher efficient catalysts for the HDS reaction.

Acknowledgement

We thank Prof. Hua Chun Zeng of National University of Singapore for fruitful discussion.

References

[1] M.G. Bawendi, M.L. Steigerwald, L.E. Brus, Annu. Rev. Phys. Chem. 41 (1990) 477.
[2] H. Weller, Angew. Chem. Int. Ed. Engl. 32 (1993) 41.
[3] S. Iijima, Nature 354 (1991) 56.
[4] P.V. Kamat, K. Vinodgopal, Langmuir 12 (1996) 5739.
[5] M.S. Rau, C.M. Kretz, L.A. Mercando, G.L. Geoffroy, A.L. Rheingold, J. Am. Chem. Soc. 113 (1991) 7420.

[6] K. Lee, W.S. Seo, J.T. Park, J. Am. Chem. Soc. 125 (2003) 3408.
[7] M. Breysse, G.D. Mariadassou, S. Pessayre, C. Geantet, M. Vrinat, G. Péro, M. Lemaire, Catal. Today 84 (2003) 129.
[8] C. Song, Catal. Today 86 (2003) 211.
[9] I.R. Moraes, M.C.P.M. Cunha, F.C. Nart, J. Braz. Chem. Soc. 7 (1996) 453.
[10] J.P. Uchida, Morishige, US patent 6,982,047 (2006).
[11] F. Shiba, M. Yokoyama, Y. Mita, T. Yamakawa, Y. Okawaa, Mater. Lett. 61 (2007) 1778.
[12] J.T. Szymanski, A.C. Roberts, Can. Miner. 22 (1984) 681.
[13] J. Livage, G. Guzman, Solid State Ionics 84 (1996) 205.
[14] X.W. Lou, H.C. Zeng, Inorg. Chem. 42 (2003) 6169.
[15] W.P. Hsu, L. Ronnquist, E. Matijevic, Langmuir 4 (1988) 31.
[16] X. Wang, Y.D. Li, J. Am. Chem. Soc. 124 (2002) 2880.
[17] L. Hnedkovsky, R.H. Wood, V.N. Balashov, J. Phys. Chem. B 109 (2005) 9034.
[18] P.H. Karpinski, J.S. Wey, J. Imaging Sci. 32 (1988) 34.
[19] T. Sugimoto, Photogr. Sci. Eng. 28 (1984) 137.
[20] S.H. Yu, B. Liu, S.M. Mao, J.H. Huang, X.M. Liu, Y.T. Qian, Adv. Funct. Mater. 13 (2003) 639.
[21] J.V. Lauritsen, S. Helveg, E. Lægsgaard, I. Stensgaard, B.S. Clausen, H. Topsøe, F. Besenbacher, J. Catal. 197 (2001) 1.
[22] P. Michaud, J.L. Lemberton, G. Pérot, Appl. Catal. A 169 (1998) 343.
[23] N.H. Topsøe, Catal. Today 130 (2008) 86.
[24] Y.D. Li, X. Li, R. He, J. Zhu, Z.X. Deng, J. Am. Chem. Soc. 124 (2002) 1411.
[25] M.V. Bollinger, J.V. Lauritsen, K.W. Jacobsen, J.V. Lauritsen, J.K. Nørskov, Phys. Rev. Lett. 87 (2001) 196803.
[26] Y. Iwata, K. Sato, T. Yoneda, Y. Miki, Y. Sugimoto, A. Nishijima, H. Shimada, Catal. Today 45 (1998) 353.
[27] Y. Iwata, Y. Araki, K. Honna, Y. Miki, K. Sato, H. Shimada, Catal. Today 65 (2001) 335.